Plasma Chemistry and Plasma Processing (2025) 45:49–68
https://doi.org/10.1007/s11090-024-10517-0

ORIGINAL PAPER

Sample Thickness and Edge Proximity Influence Spatial Behavior of Filaments and Treatment Uniformity of RF Cold Atmospheric Pressure Plasma Jet

Kateřina Polášková[1,2] · David Nečas[1] · Lukáš Dostál[3] · Miloš Klíma[4] · Lenka Zajíčková[1,2]

Received: 25 June 2024 / Accepted: 24 September 2024 / Published online: 10 October 2024

Abstract
The ability of atmospheric pressure plasma jets to treat complex non-planar surfaces is often cited as their advantage over other atmospheric plasmas. However, the effect of complex surfaces on plasma parameters and treatment efficiency has seldom been studied. Herein, we investigate the interaction of the atmospheric pressure plasma slit jet (PSJ) with block polypropylene samples of different thicknesses (5 and 30 mm) moving at two different speeds. Even though the distance between the slit outlet and the sample surface was kept constant, the treatment efficiency of PSJ ignited in the Ar and Ar/O_2 gas feeds varied with the sample thickness due to the plasma parameters such as filament count and speed being affected by the different distances of the ground (the closer the ground is, the higher the discharge electric field). On the other hand, the Ar/N_2 PSJ diffuse plasma plumes were less affected by the changes in the electric field, and the treatment efficiency was the same for both sample thicknesses. Additionally, we observed a difference in the efficiency and uniformity of the PSJ treatment of the edges and the central areas in some working conditions. The treatment efficiency near the edges depended on the duration of the filament contact, *i. e.*, how long the local electric field trapped the filaments. Conversely, the treatment uniformity near the edges and in the central areas was different if the number of filaments changed rapidly as the discharge moved on and off the sample (the 5 mm samples treated by easily sustained Ar PSJ).

Keywords Radio frequency atmospheric pressure plasma jet · Plasma filaments · Plasma treatment · Complex surfaces · Fast camera imaging

Introduction

Atmospheric pressure plasma jet (APPJ) is an overall term for discharges whose plasma extends outside the electrode arrangement into the surrounding ambience [1, 2]. The significant advantage of APPJs over other types of plasma discharges is their ability to treat complex 3D objects with non-planar surfaces. On the other hand, the diameter of the treatment area is relatively small for most APPJs, starting at 1–2 mm of kINPen [3]

Extended author information available on the last page of the article

and spanning through 10–20 mm for most capillary-based APPJs [2, 4], 15–35 mm of translational arc-discharges [5–7], 50 mm-wide quasi-2D plasma curtain jet [8], up to 150 mm of the studied RF plasma slit jet [9]. A specific type is cold APPJ, which generates plasma with no or moderate increase in neutral gas temperature. Low plasma gas temperatures are required for direct-contact biomedical applications, *i. e.*, wound healing [10, 11]. In addition, lower gas temperatures can also be beneficial for the plasma treatment of heat-sensitive materials like most synthetic polymers [2, 9].

The fundamental studies of atmospheric plasma discharges interacting with complex non-planar surfaces have recently seen an increase in interest, driven mainly by promising developments in plasma catalysis [12–14] and bioapplications [15, 16] where the interaction of discharge with such surfaces is unavoidable. Konina et al. [17] used numerical simulations to study the propagation of the surface ionization wave (SIW) across dielectric surfaces of different geometries (wavy, with cut-in pores and with water droplets on the flat surface). They showed that the negative SIW (SIW launched when the applied voltage is negative) can detach from the surface if the enhancement of the local electric field at the apex of the non-planar surface is high enough to launch a plasma ionization wave into the gas. The positive SIW, on the other hand, remains more conformal to the surface regardless of the geometry. Morsell et al. [18] used an ICCD camera to study the interaction of Ar APPJ powered by ns DC pulses with 1 kHz frequency repetition rate with a solid barrier designed as a single channel of different dimensions cut into glass slides. They observed that the SIW was less confined to the channel (*i. e.*, a higher portion of SIW escaped the channel) when its height or width was small, with the width having a slightly higher impact.

The atmospheric pressure radio-frequency (RF) plasma slit jet (PSJ) was developed by our group to remedy the APPJ issue of small treatment area size. Depending on the physical dimensions of the slit, the PSJ can produce up to 0.3 m wide cold plasma composed of self-organizing filaments extending outside the jet body. In our previous publications, we have demonstrated the uniformity of the treatment along the slit of the 150 mm-wide PSJ ignited in different gas feeds (Ar, Ar/O_2, and Ar/N_2) [19]. The feasibility of using the discharge for material treatment was proven by increased adhesion between polypropylene (PP) and the cheap epoxy adhesive with low performance in the joints with synthetic polymers [9]. During the treatment uniformity study, the modification close to the edges sometimes yielded results different from those of the central surface areas.

This work expands upon the research of the RF PSJ by investigating its treatment efficiency and uniformity near sample edges and determining which parameters cause differences between the center and edges. These differences could occur due to the local electric field enhancement at the sharp edges affecting the behavior of PSJ filaments, as observed by fast camera imaging. Gas feed (Ar, Ar/N_2, and Ar/O_2), movement speed (100 and 250 mm/s), and sample thickness (5 and 30 mm) were selected as parameters of interest. Different gas feeds were used to explore whether the influence of the local electric field on filament behavior depends on plasma gas chemistry. The treatment speed was varied to ascertain the role of filament movement. The sample thickness determined whether the filaments formed a broad base that came into contact with the edges before the vertical filaments or if they extended into the open space before moving onto the PP sample. Furthermore, the impact of sample thickness on treatment efficiency is studied for the first time. In the PSJ (and other APPJ) setups, the sample thickness governed the distance between the powered electrode and a grounded target, significantly affecting the plasma properties and, hence, the plasma treatment results.

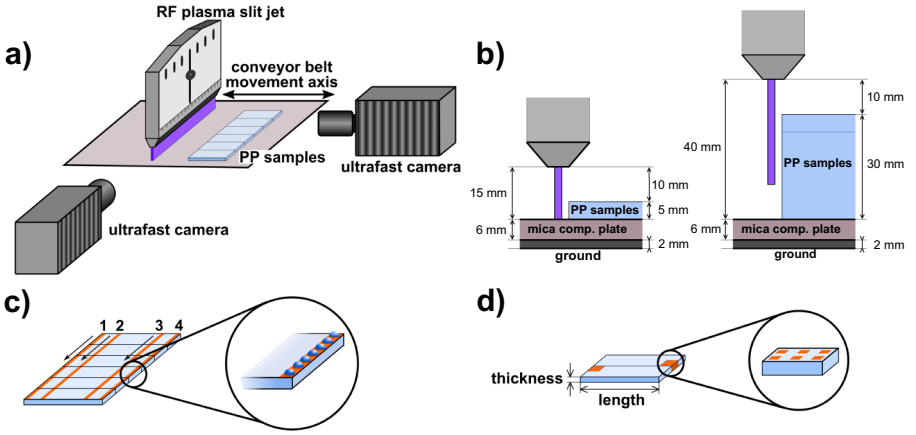

Fig. 1 **a** RF plasma slit jet experimental set-up with fast cameras positions. The dimensions are not to scale. **b** Side view of geometry for the 5–30 mm-thick sample treatment. The schemes illustrate the moment before the PSJ filaments started moving onto the samples. **c** WCAs measurement. The numbering displays the order of the sessile water droplet lines (highlighted in orange color) deposition. The arrows point in the direction of droplet deposition. **d** Placement of PP samples analyzed by XPS and the layout of measured regions (both highlighted in orange) (Color figure online)

Experimental Details

RF Plasma Slit Jet Treatment of Polypropylene

Samples of three different sizes were cut from 5 mm thick polypropylene (PP) sheets covered from both sides by the protective foil supplied under the product name PP-H Natural by the company Omniplast. The sample sizes were: 100 × 25 mm for water contact angle (WCA) measurements, 50 × 25 mm for fast camera recording, and 12.5 × 10 mm for X-ray photoelectron spectroscopy (XPS). Before the experiments, the protective foil was removed from the less rough side of the PP strips, and the surface was cleaned using the procedure described in Polášková et al. [9].

The PP strips were treated by the atmospheric pressure RF plasma slit jet (PSJ) [9, 19], a 150 mm-wide discharge composed of 7–15 self-organized filaments. Three working gas feeds were used: Ar, Ar/O_2, and Ar/N_2. The Ar flow rate was either 67 or 100 slm. The O_2 flow rate was 1 slm, and the N_2 flow rate was either 1.5 slm or 3.5 slm. The applied power of 500 or 600 W with a working frequency of 13.56 MHz was delivered by the CESAR 136 generator (Advanced Energy). The distance between the slit exit and the surface of treated PP samples was kept constant at 10 mm. During the treatment, the conveyor belt moved the samples at a constant speed of 100 or 250 mm/s. One pass was used.

The influence of sample thickness was studied using 5 mm and 30 mm thick samples placed on the dielectric mica composite plate covering the grounded conveyor belt (Figure 1b). The 5 mm is the standard thickness of the samples we used in our previous studies [9, 19]. In this configuration, the PSJ filaments remained in contact with a surface throughout treatment. The 30 mm samples represent an extreme treatment condition in which the filaments extend into the open space when not in contact with the PP sample surface. They consisted of swappable 5 mm thick PP samples placed on a 25 mm high and 250 mm wide scaffold made of PP strips.

The effect of edge proximity on treatment efficiency was monitored on sample edges parallel with the length of PSJ slit (Figure 1a), *i. e.*, on the edges through which the plasma filaments entered and left the samples. In the following text, the edge traversed by the filaments moving on the sample and the results obtained near it are referred to as the leading edge. The edge through which the filaments left the samples and the corresponding results are called the trailing edge.

Surface Characterization Methods

WCA was measured using the sessile droplet method and three-point circle (height/width) interpolation by the See System (Advex Instruments). Six PP strips placed one next to another with the shorter edges oriented parallel to the jet slit were used for one measurement (Figure 1c). Demineralized water droplets, 3 µl in volume, were deposited onto the PP surfaces in four lines parallel with the PSJ slit. The first and the last (fourth) lines of droplets were placed near the opposite sample edges, which were traversed by the plasma filaments moving on (leading edge) and off (trailing edge) the sample. The remaining two lines (lines 2 and 3 in Figure 1c) were situated in the central surface areas ~20 mm from the edges. The order in which the lines were deposited was always the same (Figure 1c). The influence of aging was ruled out using two sets of samples per one working condition that differed in the treatment direction while the order of deposited droplets was kept the same. The WCA measurement of each sample set started immediately after their plasma treatment, and it took 65 to 75 min to finish.

The obtained WCAs values were analyzed by two different approaches, yielding information about the WCAs distribution along the samples' length (*i e.*, for the four positions discussed above) and width (further in the text referred to as plasma treatment uniformity). In the former case, the mean WCA values were calculated using a maximum of 84 values – seven droplets deposited per one position (line) on a sample × six samples per sample set × two sample sets per one treatment condition. For the leading and trailing edge positions (lines 1 and 4 in Figure 1c), the WCAs monitoring the treatment uniformity along the PSJ slit length were calculated from two values (one value per sample set). For the central areas, the lines 2 and 3 were considered equal. Thus, the corresponding mean WCAs were calculated from four values.

The surface chemical composition was analyzed by XPS using the Axis Supra (Kratos Analytical) spectrometer with the monochromated Kα radiation source (Al/Ag anode). Four samples per working condition were analyzed, two on the leading and two on the trailing edge (Figure 1d). On each sample, the survey and high-resolution spectra were taken in six spots using the slot mode, collecting the signal from the area of 700 × 300 µm. Charge neutralization was used to prevent differential charging of the nonconductive samples. The survey spectra were measured using the pass energy of 80 eV with the step of 1 eV. High-resolution spectra of C, O, and N (if present) elements were recorded using the pass energy of 20 eV, step 0.1 eV, and 2–5 accumulations, the number of accumulations depending on the signal strengths. Obtained data were evaluated using CasaXPS software.

Fast Camera Imaging

Changes in the filament behavior and dynamics were investigated using two synchronized fast cameras (Figure 1a): Photron FASTCAM SA-X2 (side view) and Olympus i-SPEED 726R (front view). Both fast cameras recorded 16-bit greyscale video with the exposure

time per one frame set to 33 μs (30,000 frames/second). The remaining camera settings differed with the sample thickness (resolution) and the gas feed (shutter speed). For the 5 mm-high samples, frame resolution was 2048 × 240 px for the front-view and 896 × 368 px for the side-view video. The corresponding pixel sizes were 90 μm (front view) and 60 μm (side view). Increasing the sample thickness to 30 mm also increased the dimensions of the recorded region. Therefore, to maintain the same exposure time, the frame resolution was adjusted 1200 × 340 px for the front-view and 512 × 488 px for the side-view video. At the same time, the corresponding pixel sizes increased to 150 μm (front view) and 170 μm (side view). Different shutter speeds were used for recording Ar and Ar/O_2 PSJ discrete and Ar/N_2 diffuse filaments. For Ar and Ar/O_2 gas feeds, the shutter speed of both cameras was 5 μs. The Ar/N_2 discharge was imagined with the front-view camera set to 30 μs. The shutter speed setting of the side-view camera was 10 μs for 5 mm-high and 26.25 μs for 30 mm-high samples.

Video data from the front-view Olympus camera were processed using custom code based on Gwyddion [20] image processing libraries. The analyses focused on the filament region close to the slit exit that never overlapped with the PP samples. The processing yielded information about the mean number of filaments, their mean inter-filament distance, jitter speed (mean speed of horizontal filament movement at the frame-to-frame timescale), and several other parameters. A detailed description of the video data processing can be found in Supplementary Information of our previous publication [19]. Sometimes (open space configuration or 30 mm samples treated by Ar/O_2 and Ar/N_2 gas feeds), the light intensities of filaments were too low to be reliably detectable by the data processing. In these conditions, only the number of filaments was evaluated by manual counting.

The side-view Photron camera data were used to determine the overall duration of the treatment (referred to as the treatment time) and the time of the interaction between the PSJ filaments and the sample edges. The treatment time was determined as the time difference between the last frame before at least one filament moved onto the upper PP surface and the first frame when all the filaments left the sample. The treatment time of the edges was defined for the leading edge as the time difference between the last frame before at least one filament moved onto the upper PP surface and the first frame with all the PSJ filaments in contact with it. The same type of frames with the reverse order were used for the trailing edge.

Results and Discussion

Characteristics of RF PSJ Filaments

We have shown before that the RF PSJ interacting with thin dielectrics (6 mm mica composite) is a filamentary discharge with filaments self-organized into 1D patterns characterized by a mean inter-filament distance determined by the PSJ working conditions such as gas feed (Ar, Ar/O_2, and Ar/N_2) and applied power (500 or 600 W) [19]. Except for the filaments anchored to the slit ends and, in some working conditions, to the bump inside the slit, the PSJ filaments changed their position over time, shuffling along the length of the slit at jitter speeds dependent on the PSJ working conditions settings. Despite relatively large plasma filament separation, we demonstrated that this movement ensures excellent treatment uniformity for most PSJ settings. The choice of the gas feed also affected the discharge appearance: the Ar and Ar/O_2 filaments were thin, long, and well-defined, while the

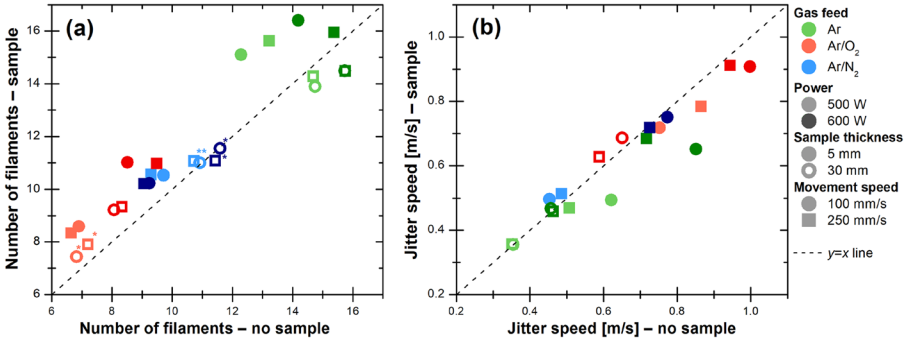

Fig. 2 The correlation between (**a**) the number and (**b**) the jitter speed of PSJ filaments when the plasma is in contact with the treated PP (the PSJ slit is 10 mm above the PP surface) and when it is not, *i. e.*, the filaments did not yet move onto the PP sample from either the mica composite substrate (in the case of 5 mm PP) or the open space configuration (in the case of 30 mm PP). Different data points represent a variety of gas feeds, RF power, sample thicknesses, and sample movement speeds. Asterisks mark the filament numbers counted manually. The Ar flow rate was 67 slm for 500 W and 100 slm for 600 W discharge. The O_2 and N_2 flow rates were 1 slm and 1.5 slm, respectively

Ar/N_2 filaments were composed of short constricted center surrounded from both sides by diffuse plasma plumes (Figure S1 in the SI).

Herein, we report on the PSJ behavior in proximity to dielectrics with different thicknesses and in open space configuration (large distance of the PSJ from the surface). In all these cases, the constricted Ar PSJ filaments appeared thin and the most numerous (Figures S1–S4 in the SI). Thermal instabilities can be responsible for the constriction of plasma into filaments [21]. According to Hofmann et al., who discussed plasma contraction in the RF APPJs, the gas temperature in the bulk should be in the order of thousand kelvin or more [22] for the thermal instability effect. The gas temperature of the PSJ, approximated by the rotational temperature calculated from the OH(A-X) spectrum, is only 740–780 K [7]. Although the OH temperature might not be a perfect representation of the gas temperature, Golubovskii's arguing that the main reason for plasma constriction in heavy noble gases is ionization non-linearity as a function of electron concentration [23] casts doubt on the explanation of the plasma constriction solely by thermal instabilities.

When ignited into an open space (40 mm between the slit outlet and mica composite on the grounded surface), the Ar plasma filaments extended relatively far outside the slit, reaching up to ~ 30 mm in length. After moving the PSJ onto 30 mm thick PP (10 mm distance between the slit outlet and the PP), the light intensity emitted by the filaments significantly increased. The light intensity also increased, although to a lesser extent, after moving the PSJ (operated 15 mm from the mica composite) above the 5 mm thick PP. On average, 13 to 16 filaments existed along the PSJ slit at the same time, depending on the working conditions (Figure 2). The mean number of filaments was slightly higher when treating the 5 mm samples, presumably due to the shorter distance (~ 21 mm) between the PSJ outlet and the ground situated beneath the mica composite plate supporting the treated PP samples.

The Ar/O_2 PSJ filaments were similar in appearance (thin and well-defined) to the Ar ones (Figures S1–S4 in the SI). An increase in filament intensity when interacting with both PP samples, 5 and 30 mm thick, was also observed for the Ar/O_2 PSJ. However, the difference between the sample and no sample configurations was less pronounced than for

Ar. The number of Ar/O_2 filaments, 7–11 per the slit length, was the lowest out of the three studied gas feeds. We attribute this decrease to a lower electron density of the Ar/O_2 plasma [19, 24], as more electrons sustaining the discharge were lost in the excitation and dissociation of molecules and electron attachments due to the electronegative character of O_2. The lower sustainability of the Ar/O_2 discharge was also the cause of short lengths (a few millimeters) of the Ar/O_2 filaments ignited to open space.

The Ar/N_2 PSJ appearance differed significantly from the other two studied gas feeds (Figures S1–S4 in the SI). Thin well-defined filaments, characteristics of the Ar and Ar/O_2 discharges, were markedly shorter in the Ar/N_2 PSJ interacting with the dielectrics, just barely appearing outside the slit. Instead, the distinguishing feature of the Ar/N_2 discharge was long diffuse plasma plumes surrounding the discrete filaments. Nitrogen molecules can form several long-lived neutral species with relatively high energies in plasma, *e. g.*, $N_2(A)$ metastables with the potential energy of 6.3 eV [25]. These species can traverse through the inhibition zone formed around the active plasma region (the central constricted filaments), into the diffuse plasma region, and, more crucially, onto the dielectric surface of the slit. There, they can induce the emission of low-energy secondary electrons that sustain the diffuse plume in a process analogous to the working principle of the homogeneous DBD in N_2 [25, 26]. The number of Ar/N_2 filaments, 9–12 per the slit length, was slightly higher than in the Ar/O_2 PSJ, suggesting slightly better sustainability of the Ar/N_2 PSJ as electrons are not lost in the electron attachments. Because the diffuse plasma plumes are composed mostly of long-lived nitrogen species, they did not terminate quickly in the open space configuration as the constricted filaments of Ar/O_2 PSJ; instead, they reached up to 25 mm in length.

Time of Filament-to-Polypropylene Interaction

The fast camera recordings were also used to evaluate the duration for which the filament bases were in contact with the different parts of the PP surface (Table 1). For the 50 mm long PP samples used during the fast camera recordings, the theoretical treatment times for which the filaments interacted with the PP sample surface were 500 and 200 ms for 100 and 250 mm/s movement speeds, respectively. Treatment times were also calculated from the fast camera recordings as the time difference between the first filament moving onto the upper PP surface (the leading edge) and the last filament leaving the sample (the trailing edge). These treatment times did not depend only on the movement speed but were also influenced by the choice of the gas feed and sample thickness and could differ from theoretical values.

The duration of Ar and Ar/O_2 PSJ filaments interaction with the surfaces of 5 mm thick samples was significantly shorter than for the 30 mm samples (compare, *e. g.*, 0.45 s for 5 mm sample to 0.63 s for 30 mm sample at 100 mm/s in Table 1). The fast camera images suggest that the difference in the treatment times stemmed from whether the filaments were ignited into the open space (for 30 mm samples) or close to dielectrics (for 5 mm samples) rather than from the influence of the exact sample thickness. Generally, the filaments should be attracted to the edges by the locally enhanced electric field, which increases their movement speed. When the Ar or Ar/O_2 PSJ was ignited against the target, its filaments formed tens of mm wide base on its surface. Thus, the edges affected the filament movement much sooner, resulting in a shorter treatment time. On the other hand, when they were ignited into the open space, the filaments were affected by the 30 mm sample presence only in the immediate vicinity of edges. Due to the lower discharge sustainability

Table 1 Interaction times between the PSJ filaments and different parts of the 50 mm long PP samples (whole surface, leading edge, trailing edge, and central areas) obtained from the fast camera recordings. The PSJ was operated in Ar (67 slm), Ar/O_2 (67/1 slm), and Ar/N_2 (67/1.5 slm) gas feeds at 500 W applied power. The distance between the slit outlet and the sample surface was 10 mm

Gas feed	Movm. speed	Changes near the edges	Treatment time (t)	Leading edge t	Trailing edge t	Treat. edges	Treat. central areas
	[mm/s]		[ms]	[ms]	[ms]	[%]	[%]
5 mm-high samples							
Ar	100	NO	450	30	28	13	87
Ar/O_2	100	NO	460	70	38	24	76
Ar/N_2	100	NO	590	47	32	13	87
Ar	250	YES	180	13	10	13	87
Ar/O_2	250	NO	190	28	17	23	77
Ar/N_2	250	YES	250	18	17	14	86
30 mm-high samples							
Ar	100	NO	630	50	37	14	86
Ar/O_2	100	NO	600	42	52	15	85
Ar/N_2	100	NO	590	37	42	13	87
Ar	250	YES	240	17	17	14	86
Ar/O_2	250	NO	260	23	28	20	80
Ar/N_2	250	YES	280	18	22	15	85

induced by the further distance to the ground, the enhancement of the local electric field at the edges ensnared the filaments, prolonging the treatment time slightly over the theoretical values. Furthermore, the leading edge seems to repel the filaments, presumably due to the changes in the flow patterns. As a result, filaments struggled to climb onto the upper surface, which could have also contributed to the treatment time increase (Table 1).

In the Ar/N_2 PSJ, the treatment times obtained by the analysis of fast camera videos were more or less the same for both sample thicknesses (Table 1). Unlike the Ar and Ar/O_2 PSJ treatment carried out by constricted 'active' plasma filaments affected by the different sample thicknesses, only the diffuse parts of plasma filaments interacted with the PP sample surface during the Ar/N_2 treatment. We expect the diffuse plasma plumes to have much lower electron density than constricted plasma because they are composed mainly of neutral nitrogen species and low-energy secondary electrons (the probability of them inducing volumetric ionization reaction is low) emitted from the dielectric surface of the slit by the said species. Therefore, the locally enhanced electric field at the sample edges had little to no influence on the Ar/N_2 PSJ filament behavior, and no change in treatment times was observed between the samples of different thicknesses.

The choice of the gas feed also affected the time for which the plasma filament bases interacted with the sample edges, determined as the time difference between the last frame with no filament in contact with the upper PP surface and the first frame with all the PSJ filaments in contact with it, and vice versa depending on the edge. Out of the three studied gas feeds, the Ar/O_2 plasma filaments stayed in contact with the sample edges longer, 20–24% of the overall treatment time, that in Ar and Ar/N_2 (13–15%). We assume the locally enhanced electric field could keep the Ar/O_2 plasma filaments in contact with the edges longer because of the lower discharge sustainability. On the other hand, the easily

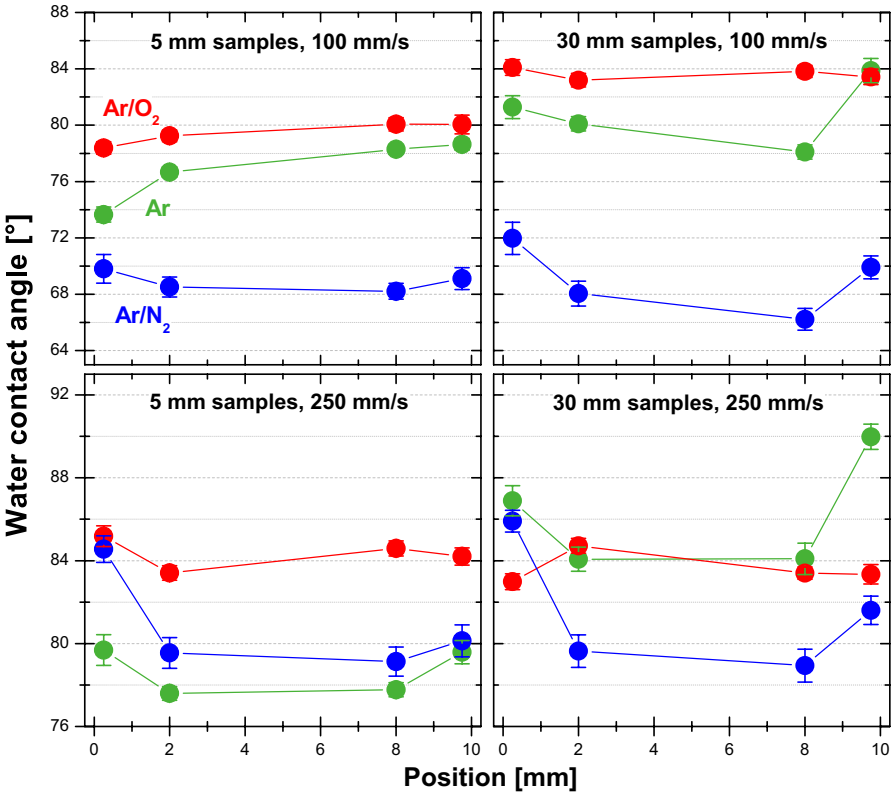

Fig. 3 Mean values of water contact angles measured after Ar, Ar/O_2, and Ar/N_2 plasma treatment at two treatment speeds at different positions along the PP samples (total length of 10 mm) of two different thicknesses (5 and 30 mm). The PSJ discharge parameters were 500 W of applied RF power, 67 slm of Ar flow rate, and, when using the gas mixtures, 1 slm of oxygen or 1.5 slm of nitrogen. The distance between the PSJ slit outlet and the sample surface was kept at 10 mm. The WCA of untreated PP was (101 ± 1)°

sustained Ar PSJ filaments could escape the locally enhanced electric field without much issue, and the Ar/N_2 low electron density diffuse filaments remained unaffected.

Parameters Influencing Plasma Treatment Efficiency

The efficiency of plasma treatment, herein evaluated by the degree of surface wettability and the concentration of functional groups (Figures 3 and 4), was affected by all tested parameters, *i. e.*, gas feed, treatment speed, and sample thickness. The plasma-induced changes in the surface topography that can potentially influence the wettability measurements were considered negligible because, in our previous work using a confocal microscope, we did not observe any difference between the surface topography before and after the plasma treatment even when the treatment time was 45×/115× longer than here [9]. Using AFM to measure the topography changes is not feasible due to the high initial variety in our samples' roughness.

The treatment speed influence is straightforward: faster conveyor belt speed led to a lower interaction time of plasma filaments per unit surface area regardless of the gas feed

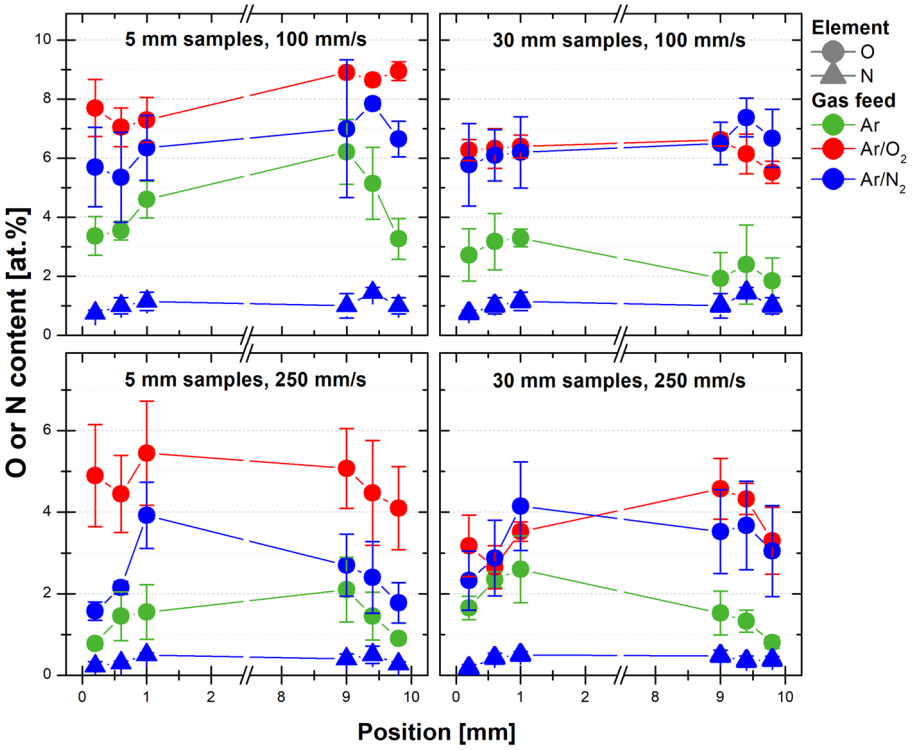

Fig. 4 Mean values of O and N content (C + O + N = 100 at.%) measured after Ar, Ar/O_2, and Ar/N_2 plasma treatment at two treatment speeds at different positions along the PP samples (total length of 10 mm) of two different thicknesses (5 and 30 mm). The untreated PP sample contained no functional group, *i. e.*, both O and N contents were zero. The plasma treatment in Ar and Ar/O_2 did not introduce any nitrogen

(Table 1). Thus, fewer functional groups were attached to the PP surface, resulting in a less pronounced decrease in wettability. The WCA obtained on samples treated at 250 mm/s were up to 11° higher than when the lower movement speed was used (Figure 3). Correspondingly, on average, the O and N content representing the newly attached functional groups was lower by 2–4 at.% (Figure 4).

The gas feed choice affected the plasma gas composition [9] and thus also the concentration of gaseous reactive species interacting with the sample surface. As the gaseous reactive species (O, OH, N, $N_2(A)$, H, O_2^*, O_3, ...) have different reactivity with the PP chain [27], the PSJ treatment efficiency will inherently differ for different gas feeds. The choice of the gas feed also determined whether the sample thickness affected the treatment time (Table 1) and, thus, the results. Therefore, both parameters are discussed together.

According to the WCA results (Figure 3), the efficiency of the Ar/N_2 PSJ treatment was commonly the highest among the three tested gas feeds. It was also the only treatment whose results were independent of sample thickness. The obtained WCAs were cca 68° for 100 mm/s treatment speed and 79° for 250 mm/s. The Ar PSJ treatment efficiency has decreased with the faster movement speed and increased sample thickness. The mean WCAs increased from 77° measured for the 5 mm samples treated at 100 mm/s movement speed to 84° corresponding to the 30 mm high samples treated at 250 mm/s. The Ar/O_2 PSJ

treatment was the least efficient (according to the WCAs results) and least affected by the movement speed and sample thickness choices, with the mean WCAs ranging from 80 to 84°. To better understand these results, the fast cameras were used to record the front and side view of the interaction between the plasma filaments and the PP surface (Figure 1).

As discussed in subsection 3.1, the RF PSJ discharge consisted of filaments self-organized into patterns characterized by the mean inter-filament distance (number of filaments) dependent on the working conditions settings. For the Ar PSJ, the number of filaments, their jitter speed, and treatment time derived from fast camera recordings all differed with the sample thickness. The number of filaments (15–15.5 compared to 14) and their jitter speed (0.48 m/s compared to 0.36 m/s) was higher when treating 5 mm, compared to 30 mm thick samples (Figure 2). On the other hand, the treatment times were slightly longer for the 30 mm samples, *e. g.*, 630 ms compared to 450 ms for 50 mm long samples moved at 100 mm/s (Table 1). Because the WCAs were lower for thinner samples, we can conclude that the number of Ar filaments and their jitter speed have a higher impact in determining the treated PP surface wettability than the treatment time. The less pronounced influence of treatment time is further demonstrated by no or minor differences between the WCAs obtained on samples with the same thicknesses treated at 100 and 250 mm/s (Figure 3). For the 5 mm samples, a slight increase in the number of filaments from 15 to 15.6 seems to have compensated for the lower treatment times, as WCAs obtained for 100 and 250 mm/s movement speeds were the same. As for the 30 mm samples, there is no difference between the number of filaments interacting with the PP surface at different movement speeds, and the WCA values were slightly higher at 250 m/s.

The sample thickness affected the filament count and movement by changing the distance between the jet and the grounded conveyor belt. When treating the thinner sample, the ground proximity enhanced the macroscopic electric field of the discharge [28] and, hence, its sustainability. The higher number of filaments improved treatment efficiency by increasing the area treated at a given moment. Furthermore, the macroscopic electric field enhancement likely led to an increase in the electron density of plasma filaments and, thus, in the higher concentration of reactive species, contributing to improved treatment efficiency. Jitter speed is a motion characteristic encompassing both the shuffling of filaments along the length of the slit and their self-organizing nature, *i. e.*, the movement induced by the random formation and decay events. Thus, even though it was computed using the well-distinguishable upper parts of filaments, it can be used as a proxy for the filament base motion. At the higher speed, filaments covered more distance, increasing the chance of the area being treated several times and hence treatment efficiency.

The changes in wettability of 5 and 30 mm thick PP samples induced by the Ar/O_2 PSJ treatment followed the same trends as for the Ar PSJ treatment: the mean WCAs of Ar/O_2 -treated PP were slightly higher at the 30 mm samples, as were the treatment times (0.60 s compared to 0.47 s for 50 mm long samples moved at 100 mm/s). The filament count was lower when treating the 30 mm samples (7.5–8 compared to 8–8.5 for 5 mm samples), resulting in the slightly higher WCAs. The jitter speed was not estimated for the 30 mm sample and 500 W applied power (the conditions at which the WCAs from the Figure 3 were obtained) because the Ar/O_2 plasma filaments were too short and dim for the analysis to yield any reliable results. Nonetheless, based on the values obtained for the Ar/O_2 discharge ignited at 600 W (Figure 2), we presume that the jitter speed of the 500 W Ar/O_2 discharge was significantly lower when treating the 30 mm samples, thus also contributing to the slightly higher WCAs.

The Ar/N_2 plasma treatment-induced change in the PP surface wettability was the only one out of the three studied gas feeds independent of sample thickness (Figure 3). The

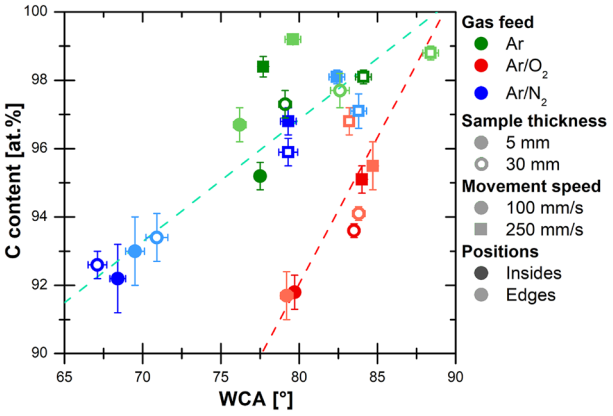

Fig. 5 Correlation between the WCAs and C content (C + O + N = 100 at.%) obtained by XPS for different gas feeds, sample thicknesses, movement speeds, and positions on the PP sample surface

Ar/N_2 modification was carried out by the diffuse part of plasma filaments composed mainly of neutral long-lived reactive species and low-energy secondary electrons. Therefore, their properties were less influenced (the number of filaments was the same 10–11 when the PSJ impinged on a surface) by changes in the electric field brought on by either the distance between the slit outlet and the ground situated beneath the substrate carrying samples or the sample edges. On the other hand, the movement speed, which had a moderate effect on the Ar and Ar/O_2 PSJ-induced wettability changes, significantly impacted the Ar/N_2 results. The mean WCAs increased from 68° to 79° when the movement speed was increased (Figure 3), even though the filament number was higher at the 250 mm/s (9 filaments compared to 10.5 filaments as seen in Figure 2a). The larger number of filaments not being able to compensate for the shorter treatment time presumably stems from the diffuse character of Ar/N_2 plasma that had a lower concentration of reactive oxygen and nitrogen species capable of affecting the PP chains [9, 27]. Additionally, the smaller filament base width (10 mm compared to ~30 mm of Ar and Ar/O_2 PSJ as seen in Figures S1 and S2 in the SI) could also be a contributing factor.

As discussed above, the PSJ treatment attached new functional groups to the PP sample surface, which were solely responsible for the wettability increase because the changes in topography were unlikely at the studied treatment times. Thus, the lowest WCAs should roughly correspond to the highest concentration of functional groups. However, that was not always the case for our results (see Figures 3 and 4), with the Ar/O_2 data standing out the most. Out of the three studied gas feeds, the Ar/O_2 PSJ treatment led to the lowest increase in wettability. In contrast, its O content, representing the newly attached oxygen functional groups, was the highest.

The correlation of the WCAs and C content (Figure 5) revealed that the Ar/O_2 PSJ affected the PP surface differently from the Ar and Ar/N_2 discharges. Two causes for the trend or their combination are possible. Functional groups attached by the Ar/O_2 treatment could be more concentrated below the topmost surface layer, either due to the higher penetration depth of the treatment or due to the surface-oriented functional groups rotating into the PP bulk immediately after the treatment. The former possibility is somewhat supported by the results of Abou Rich et al. [29] who reported higher oxygen penetration depths into the low-density polyethylene when the sample was treated in Ar/O_2 atmospheric post-discharge than in the Ar post-discharge. Alternatively, the Ar/O_2 PSJ could have changed the PP surface topography in the plasma-polymer etching process [30], which would have

influenced the measured WCAs but not on the XPS (information depth of 5 nm). However, this possibility is less likely, as we do not expect any surface topography changes to occur during the PSJ plasma treatment for the reasons discussed at the beginning of this section.

Plasma Treatment Efficiency at the Sample Edges

In some working conditions, both the WCA (Figure 3) and XPS (Figure 4) results varied with the positions along the treated sample length, especially in the sample edges proximity. Because the differences are relatively small (the changes in the elemental compositions are often within measurement errors), we used Fisher's method [31] to combine the *p*-values for the individual measurements. Specifically, the four *p*-values corresponding to (WCA, XPS) and (leading, trailing) combinations, obtained using Welch's unequal variances *t*-test [32], were always used for a combined probability test whether the edge and center data differ.

Of the three studied gas feeds, the Ar/O_2 PSJ treatment was the only one unaffected by the edges with the mean WCAs and elemental compositions constant over the whole 100 mm length of PP sample for all the combinations of sample thickness and treatment speed (Figures 3 and 4). The comparison of treatment times determined from the fast camera videos explains why. The Ar/O_2 PSJ filaments interacted with both leading and trailing edges for longer time than the filaments of the PSJ ignited in Ar and Ar/N_2 gas feeds (Table 1). It ensured the edges were sufficiently treated even at 250 mm/s treatment speed.

The Ar PSJ treatment efficiency typically decreased (functional group concentration was lower and the WCA was higher) in the vicinity of edges, with the trailing edge having a slightly more pronounced influence. The lower treatment efficiency correlates with shorter plasma exposure, as illustrated by the lower percentage of overall treatment time filaments spent in contact with edges (Table 1). The exception was the results obtained at the leading edge of 5 mm sample (Figure 3). The mean WCA at this position, 74°, was lower compared to the cca 78° of the central samples area, suggesting a higher concentration of functional groups. However, the XPS results show a slight decrease in the functional group content (Figure 4) near both edges. The origin of these conflicting data lies in the unique behavior of Ar filaments in this configuration. The long base of Ar filaments, formed on the mica substrate surface, could climb along the PP sample sides, even reaching out above the upper surface (Figure 6), which was not observed in other conditions. The long-lived reactive species (OH radicals, nitrogen metastables, ...) left after the above surface-reaching filament base could diffuse onto the surface of the PP edge, treating it before the arrival of filaments. However, this kind of treatment is very mild, explaining why its effects are observable only by the topmost-surface sensitive WCAs measurement.

In contrast to Ar and Ar/O_2 PSJ, the influence of edge proximity on the Ar/N_2 treatment efficiency differed with the working conditions. The WCA and XPS results were constant over the whole length of 5 mm sample treated at 100 mm/s. On the other hand, the Ar/N_2 treatment efficiency decreased near the edges of 30 mm samples due to a slightly higher degree of treatment non-uniformity, presumably resulting from the sample leading side acting as a wall disrupting the flow patterns. At the faster movement speed of 250 mm/s, the Ar/N_2 treatment efficiency differed near the edges of PP samples of both thicknesses (Figures 3 and 4). This change was significantly larger (WCA increased by up to 5–6°, O and N content decreased by 2–3 at.%) than in the Ar PSJ (WCA increased at the edges by 3–4° and O content decreased by 0.5–1.5 at.%) despite the percentage of treatment time the filaments stayed in contact with the edges being the same for both gas feeds (13–15% for

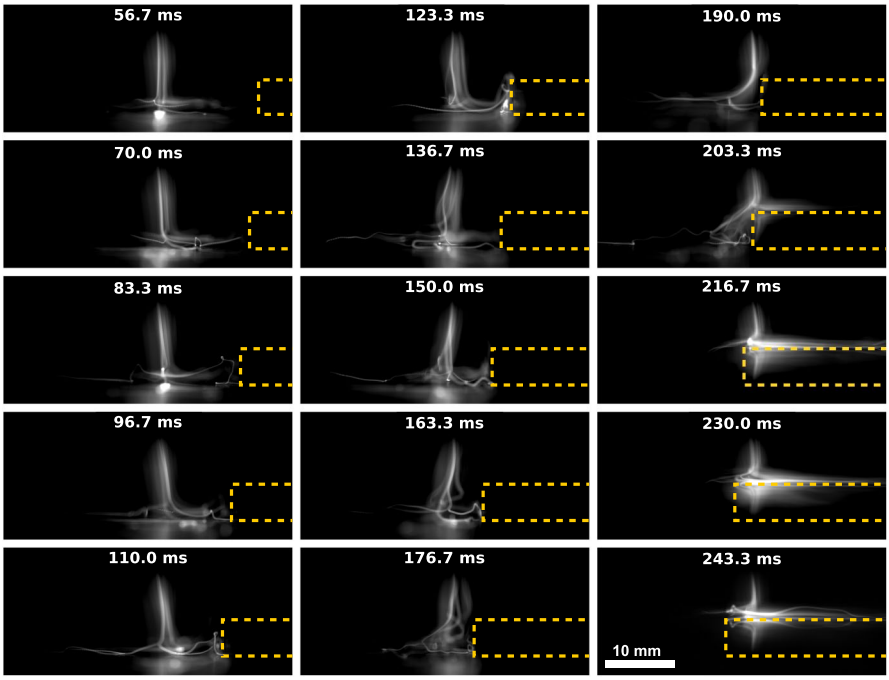

Fig. 6 Side-view fast camera images (with sample outline indicated by a yellow dashed line), taken with 33.3 µs exposure time, of Ar PSJ (67 slm Ar, 500 W) filaments interacting with the leading edge of 5 mm PP sample moved 100 mm/s. The distance between the slit outlet and the substrate covering the conveyor belt was 15 mm. The fast camera was set to look at the sample from a slight upper angle, slightly distorting the *y*-dimension scale (Color figure online)

the Ar/N_2 filaments compared to 13–14% for the Ar PSJ). The most probable cause of the steep decrease in the Ar/N_2 PSJ treatment efficiency is the significantly shorter width of the filament base that was not accounted for during the treatment time determinations. Considering the different base widths, the Ar/N_2 filaments were in contact with the edges for a shorter time than Ar PSJ filaments, despite the leading and trailing edge treatment times being the same or even slightly longer for the Ar/N_2 PSJ (Table 1), explaining the observed steeper decrease in treatment efficiency.

Treatment Uniformity Along the PSJ Slit

In our previous publication [19], we have shown that the PSJ treatment uniformity along the slit differs with the gas feed and, to a lesser degree, with the treatment speed. Thus, the question of whether uniformity also depends on sample thickness or edge proximity (as was the case for average treatment efficiency) arose.

The plasma treatment of the central PP surface areas by the Ar discharge was more or less uniform along the jet slit in all the studied conditions (Figure 7), although the error bars of the mean WCAs were notably higher at the 30 mm samples. It was presumably a consequence of the lower average number of Ar PSJ filaments interacting with the 30 mm sample (Figure 2), caused by the ground being further away from the slit resulting in the lower macroscopic electric field [28]. In addition to larger error bars, the WCAs of 30 mm

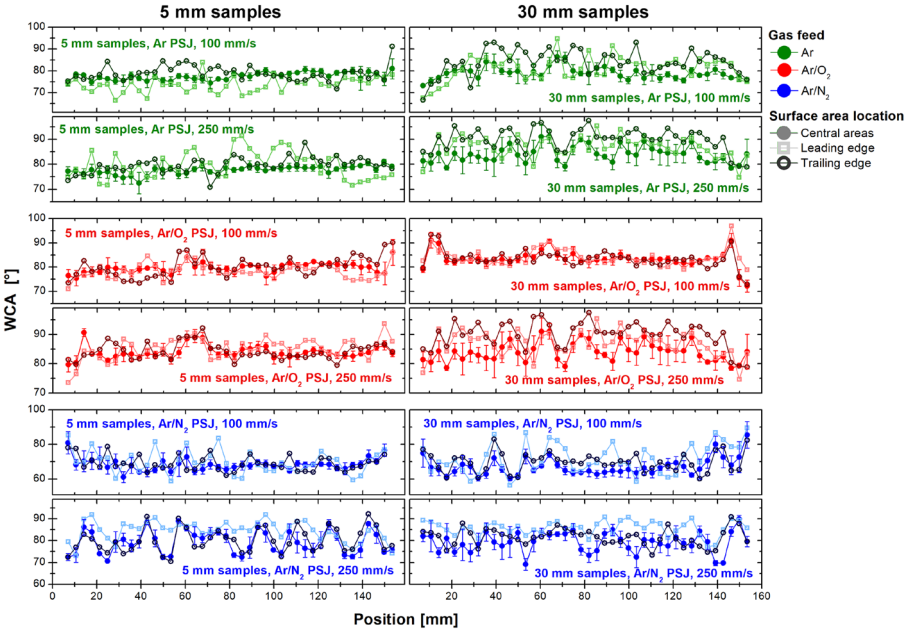

Fig. 7 Dependence of water contact angle on the position along the jet slit for different locations on the surface of the 5 and 30 mm thick PP samples treated by the PSJ ignited in different gas feeds

samples treated by the Ar PSJ fluctuated slightly around 60 mm. In this position, the local PSJ electromagnetic field was higher due to a slight bump in the otherwise uniformly distanced slit. As a result, jittering plasma filaments were often trapped here, forcing the other filaments to rearrange to maintain a characteristic inter-filament distance [19]. In the lower electric fields (30 mm sample treatment), sustaining the discharge was more difficult, filaments moved less, and they were more easily attached to the favorable positions (bump, slit ends), hence the lower treatment uniformity around 60 mm position.

Edge proximity affected the Ar PSJ treatment uniformity only for the 5 mm samples (Figure 7). The slight variations observed for the 30 mm samples resulted from the inherently lower uniformity of the treatment rather than the edge influences. The effect of the edges on the uniformity of Ar PSJ treatment was connected to the changes in the number of filaments. For the 5 mm sample, the filament count increased and decreased rapidly (Figure 8) when the discharge moved on and off the sample and hence the observed difference in the treatment uniformity near the edges. On the other hand, the number of filaments did not change during the discharge transition from the open space to the 30 mm samples. Thus, no significant difference in the uniformity was observed.

The Ar/O_2 treatment was less uniform than the Ar PSJ modification. In addition to the less treated area around 55–75 mm caused by a bump inside the slit trapping the filaments in a fixed position, two peaks in WCAs values near the ends of the position range were sometimes observed. They originated from the stationary long-lived (lifetimes longer than the treatment duration) filaments formed at the slit ends. The uniformity of the 30 mm sample treated at 250 mm/s was notably lower than that of the other Ar/O_2-treated samples due to a combination of shorter treatment time with fewer longer-lived partly static filaments. The edges did not observably affect the Ar/O_2 PSJ treatment uniformity (Figure 8). The

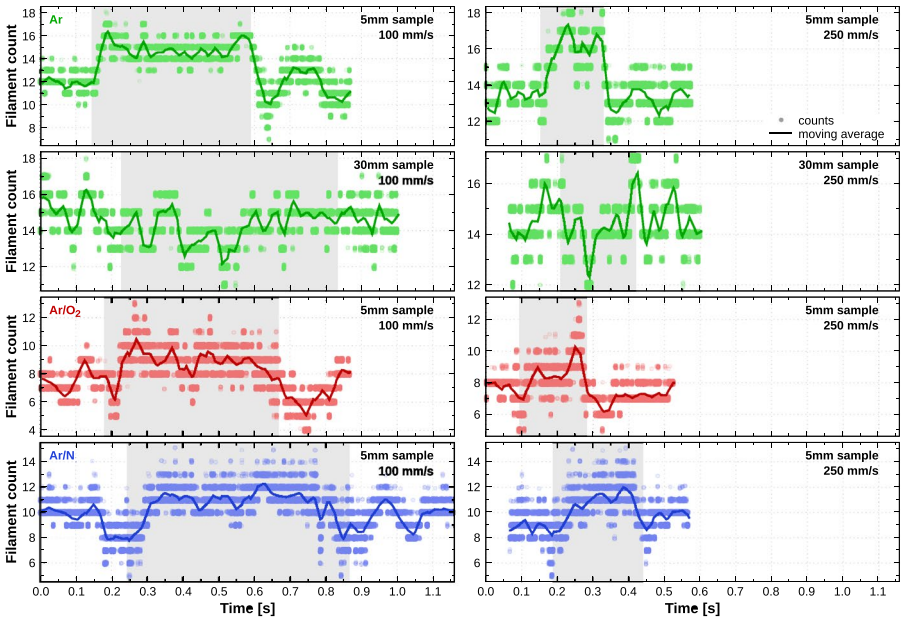

Fig. 8 Time evolution of the number of PSJ filaments during their interaction with the PP samples (gray background) of different thicknesses moving at 100 (left column) and 250 mm/s (right column). The applied power was 500 W, Ar flow rate was kept at 67 slm in all the PSJ settings, N_2 and O_2 flow rates were 1.5 and 1 slm

WCAs corresponding to a specific position along the PSJ slit were the same in all three distinct surface regions (edges and central area). Similar to the Ar PSJ, the impact of edge proximity on the treatment uniformity could be correlated to the change in the number of filaments when the PSJ moved on and off the sample. The Ar/O_2 filament count was mostly unaffected by the transition between the two different surface thicknesses. Thus, the treatment uniformity along the slit length was the same in all the surface regions.

According to the WCA results (Figure 7), the Ar/N_2 PSJ treatment was relatively uniform along the slit at 100 mm/s movement speed and nonuniform at 250 mm/s. However, as we have shown in our previous publication [19], the treatment was, in reality, nonuniform at both speeds, with the less-treated areas (2–5 mm in diameter) at the positions of dark regions in between the individual filaments. At 100 mm/s, the treatment time was long enough compared to the travel speed of filaments along the slit that the averaging of the results from the central areas (four values) erased most of the nonuniformities. On the other hand, the mean WCAs of the leading and trailing edges were calculated from only two values and hence their occasional difference. At 250 mm/s, the treatment time was too low to be compensated by filament movement, resulting in highly nonuniform modification with pronounced differences between the edges and central area. The number of filaments changed marginally when the discharge moved on and off the sample (Figure 8). Therefore, the different treatment uniformity at the edges can be mainly attributed to the different and unaveraged positions of the filaments along the slit. For the 30 mm samples, the results were also affected by the reduced filament stability caused by the changes in the flow pattern due to the sample acting as a solid obstacle.

In summary, edge proximity had a significant influence on treatment uniformity only for the 5 mm samples modified by the Ar PSJ whose filament count responded quickly (0.03–0.07 s) to the sample's presence (and removal). This rapid change in the number of filaments occurred only in these experimental settings due to the excellent sustainability of the Ar discharge, further enhanced by the proximity of the ground increasing the PSJ electric field [28]. While the electric field of Ar/O_2 and Ar/N_2 PSJ was also enhanced in the proximity of the ground, the discharges were not as easily sustained due to the loss of electrons in dissociation and excitation of molecules or by attachment to the electronegative oxygen. Thus, the change of the distance between the slit exit and a substrate, had little impact on the number of Ar/O_2 and Ar/N_2 filaments, resulting in the same treatment uniformity of both central area and edges.

Conclusion

The RF plasma slit jet (PSJ) ignited in three different gas feeds (Ar, Ar/O_2, and Ar/N_2) was used to treat PP samples of two different thicknesses (5 and 30 mm) moved with 100 and 250 mm/s speed. All three parameters (gas feed, sample thickness, and movement speed) affected the PSJ treatment efficiency. Gas feed had the largest impact. Igniting the PSJ into an open space (treatment of 30 mm samples) reduced the discharge sustainability. For Ar and Ar/O_2 discharges, it led to a decrease in the number of filaments, the jitter speed at which they shuffle along the slit, and presumably the lower concentration of reactive species. On the other hand, the treatment time determined from the fast camera recordings was slightly shorter for the thinner samples because the long bases of constricted Ar and Ar/O_2 filaments, formed on the surface of the mica composite dielectric covering the conveyor belt, were pulled towards the sample edges by the higher local electric field. The higher plasma sustainability was the dominant factor determining the treatment efficiency evaluated by the WCA and XPS results as it was higher at 5 mm samples despite the shorter duration of Ar and Ar/O_2 filament contact.

The Ar/N_2 PSJ treatment was carried out by diffuse plasma plumes composed of mostly neutral long-lived nitrogen species and low-energy electrons. Therefore, the influence of the locally enhanced electric field at the sample edges was minimal, and the treatment times and efficiency was the same for the samples of both thicknesses. Conversely, the Ar/N_2 plasma composition (the nitrogen gas species have much lower reactivity with PP than the oxygen ones) combined with the narrow filament base led to a steep decrease in the treatment efficiency at the higher movement speed.

The efficiency and uniformity of the PSJ treatment differed between the edges and the central areas in some working conditions. The treatment efficiency near the edges depended on the duration of the filament contact. The Ar/O_2 PSJ filaments stayed affixed to the sample edges for a higher percentage of the overall treatment time, ensuring the same treatment efficiency of all the surface areas. On the other hand, the easily sustained Ar filaments and diffuse Ar/N_2 filaments left the edges after a shorter contact. At 250 mm/s, the contact was too short, and the treatment was less efficient close to the edges. The treatment uniformity near the edges and in the central areas differed if the number of filaments changed rapidly as the discharge moved on and off the sample (the 5 mm samples treated by Ar PSJ).

Supplementary Information The online version contains supplementary material available at https://doi.org/10.1007/s11090-024-10517-0.

Author contributions Conceptualization: K.P. and L.Z; Methodology: K.P., L.D. and L.Z.; Software: D.N.; Validation: K.P.; Formal Analysis: K.P. and D.N.; Investigation: K.P., L.D. and M.K.; Resources: M.K.; Writing – Original Draft Preparation: K.P.; Writing – Review & Editing: K.P., D.N. and L.Z.; Visualization: K.P. and D.N.; Supervision: L.Z.

Funding Open access publishing supported by the National Technical Library in Prague. This work has been supported by the Czech Science Foundation in the frame of project 20-14105S. CzechNanoLab project LM2023051 funded by MEYS CR is gratefully acknowledged for the financial support of the measurements/sample fabrication at CEITEC Nano Research Infrastructure.

Declarations

Conflict of interest The authors declare no Conflict of interest.

Ethic approval Not applicable

References

1. Winter J, Brandenburg R, Weltmann K (2015) Atmospheric pressure plasma jets: an overview of devices and new directions. Plasma Sour Sci Technol 24(6):064001. https://doi.org/10.1088/0963-0252/24/6/064001
2. Kostov KG, Nishime TMC, Castro AHR, Toth A, Hein LRdO (2014) Surface modification of polymeric materials by cold atmospheric plasma jet. Appl Surf Sci 314:367–375. https://doi.org/10.1016/j.apsusc.2014.07.009
3. Reuter S, Woedtke T, Weltmann K-D (2018) The kINPen—a review on physics and chemistry of the atmospheric pressure plasma jet and its applications. J Phys D: Appl Phys 51(23):233001. https://doi.org/10.1088/1361-6463/aab3ad
4. Weltmann KD, Brandenburg R, Woedtke T, Ehlbeck J, Foest R, Stieber M, Kindel E (2008) Antimicrobial treatment of heat sensitive products by miniaturized atmospheric pressure plasma jets (APPJs). J Phys D: Appl Phys 41(19):194008. https://doi.org/10.1088/0022-3727/41/19/194008
5. Jelínek P, Polášková K, Jeník F, Jeníková Z, Dostál L, Dvořáková E, Cerman J, Šourková H, Buršíková V, Špatenka P et al (2019) Effects of additives on atmospheric pressure gliding arc applied to the modification of polypropylene. Surf Coat Technol 372:45–55. https://doi.org/10.1016/j.surfcoat.2019.04.035
6. Kehrer M, Rottensteiner A, Hartl W, Duchoslav J, Thomas S, Stifter D (2020) Cold atmospheric pressure plasma treatment for adhesion improvement on polypropylene surfaces. Surf Coat Technol 403:126389. https://doi.org/10.1016/j.surfcoat.2020.126389
7. Polášková K, Ozkan A, Klíma M, Jeníková Z, Buddhadasa M, Reniers F, Zajíčková L (2023) Comparing efficiencies of polypropylene treatment by atmospheric pressure plasma jets. Plasma Process Polym 20(11):2300031. https://doi.org/10.1002/ppap.202300031
8. Richards C, Jans E, Gulko I, Orr K, Adamovich IV (2022) N_2 vibrational excitation in atmospheric pressure ns pulse and rf plasma jets. Plasma Sour Sci Technol 31(3):034001. https://doi.org/10.1088/1361-6595/ac4de0
9. Polášková K, Klíma M, Jeníková Z, Blahová L, Zajíčková L (2021) Effect of low molecular weight oxidized materials and nitrogen groups on adhesive joints of polypropylene treated by a cold atmospheric plasma jet. Polymers 13(24):4396. https://doi.org/10.3390/polym13244396

10. Cheng K-Y, Lin Z-H, Cheng Y-P, Chiu H-Y, Yeh N-L, Wu T-K, Wu J-S (2018) Wound healing in streptozotocin-induced diabetic rats using atmospheric-pressure argon plasma jet. Scientific reports 8(1):12214. https://doi.org/10.1038/s41598-018-30597-1
11. Bekeschus S, Woedtke T, Emmert S, Schmidt A (2021) Medical gas plasma-stimulated wound healing: evidence and mechanisms. Redox Biol 46:102116. https://doi.org/10.1016/j.redox.2021.102116
12. Chen G, Snyders R, Britun N (2021) CO_2 conversion using catalyst-free and catalyst-assisted plasma-processes: recent progress and understanding. J CO2 Utilization 49:101557. https://doi.org/10.1016/j.jcou.2021.101557
13. Salden A, Budde M, Garcia-Soto CA, Biondo O, Barauna J, Faedda M, Musig B, Fromentin C, Nguyen-Quang M, Philpott H et al (2023) Meta-analysis of CO_2 conversion, energy efficiency, and other performance data of plasma-catalysis reactors with the open access PIONEER database. J Energy Chem 86:318–342. https://doi.org/10.1016/j.jechem.2023.07.022
14. Hinshelwood M, Oehrlein GS (2023) Plasma catalysis: separating plasma and surface contributions for an $Ar/N_2/O_2$ atmospheric discharge interacting with a Pt catalyst. Plasma Sour Sci Technol 32(12):125001. https://doi.org/10.1088/1361-6595/ad0f47
15. Janů L, Dvořáková E, Polášková K, Buchtelová M, Ryšánek P, Chlup Z, Kruml T, Galmiz O, Nečas D, Zajíčková L (2023) Enhanced adhesion of electrospun polycaprolactone nanofibers to plasma-modified polypropylene fabric. Polymers 15(7):1686. https://doi.org/10.3390/polym15071686
16. Kong X, Li S, Li H, Yang W, Yang D, Ning W, Wang R (2023) Distribution patterns of reactive species in the interaction between atmospheric pressure plasma jet and fiber membrane. Plasma Sour Sci Technol 32(10):105004. https://doi.org/10.1088/1361-6595/acfd5b
17. Konina K, Kruszelnicki J, Meyer ME, Kushner MJ (2022) Surface ionization waves propagating over non-planar substrates: wavy surfaces, cut-pores and droplets. Plasma Sour Sci Technol 31(11):115001. https://doi.org/10.1088/1361-6595/ac9a6c
18. Morsell J, Trosan D, Stapelmann K, Shannon S (2023) Plasma surface ionization wave interactions with single channels. Plasma Sour Sci Technol 32(9):095017. https://doi.org/10.1088/1361-6595/acf9c9
19. Polášková K, Nečas D, Dostál L, Klíma M, Fiala P, Zajíčková L (2022) Self-organization phenomena in cold atmospheric pressure plasma slit jet. Plasma Sour Sci Technol 31(12):1–13. https://doi.org/10.1088/1361-6595/acab82
20. Nečas D, Klapetek P (2012) Gwyddion: an open-source software for SPM data analysis. Cent Eur J Phys 10:181–188. https://doi.org/10.2478/s11534-011-0096-2
21. Fridman A (2008) Electric discharges in Plasma Chemistry. In: Fridman A (ed) Plasma chemistry. Cambridge University Press, New York
22. Hofmann S, Van Gessel A, Verreycken T, Bruggeman P (2011) Power dissipation, gas temperatures and electron densities of cold atmospheric pressure helium and argon RF plasma jets. Plasma Sour Sci Technol 20(6):065010. https://doi.org/10.1088/0963-0252/20/6/065010
23. Golubovskii YB, Nekuchaev V, Gorchakov S, Uhrlandt D (2011) Contraction of the positive column of discharges in noble gases. Plasma Sour Sci Technol 20(5):053002. https://doi.org/10.1088/0963-0252/20/5/053002
24. Park G, Lee H, Kim G, Lee JK (2008) Global model of He/O_2 and Ar/O_2 atmospheric pressure glow discharges. Plasma Process Polym 5(6):569–576. https://doi.org/10.1002/ppap.200800019
25. Massines F, Ghérardi N, Naudé N, Ségur P (2009) Recent advances in the understanding of homogeneous dielectric barrier discharges. Eur Phys J-Appl Phys. https://doi.org/10.1051/epjap/2009064
26. Massines F, Sarra-Bournet C, Fanelli F, Naudé N, Gherardi N (2012) Atmospheric pressure low temperature direct plasma technology: status and challenges for thin film deposition. Plasma Process Polym 9(11–12):1041–1073. https://doi.org/10.1002/ppap.201200029
27. Dorai R, Kushner MJ (2003) A model for plasma modification of polypropylene using atmospheric pressure discharges. J Phys D: Appl Phys 36(6):666. https://doi.org/10.1088/0022-3727/36/6/309
28. Polášková K, Drexler P, Klíma M, Macháč J, Nečas D, Švanda M, Zajíčková L (2024) Electric field and higher harmonics of RF plasma slit jet measured by antennas and VI probes. Plasma Sour Sci Technol 33(5):055017. https://doi.org/10.1088/1361-6595/ad48b5
29. Abou Rich S, Leroy P, Dufour T, Wehbe N, Houssiau L, Reniers F (2014) In-depth diffusion of oxygen into LDPE exposed to an $Ar\text{-}O_2$ atmospheric post-discharge: a complementary approach between AR-XPS and Tof-SIMS techniques. Surf Interface Anal 46(3):164–174. https://doi.org/10.1002/sia.5403
30. Luan P, Knoll AJ, Bruggeman PJ, Oehrlein GS (2017) Plasma-surface interaction at atmospheric pressure: A case study of polystyrene etching and surface modification by Ar/O_2 plasma jet. J Vac Sci Technol 10(1116/1):5000691
31. Fisher RA (1970) Statistical methods for research workers. Breakthroughs in Statistics: Methodology and Distribution. Springer, Berlin, pp 66–70

32. Welch BL (1947) The generalization of 'Student's' problem when several different population variances are involved. Biometrika 34:28–35. https://doi.org/10.1093/biomet/34.1-2.28

Authors and Affiliations

Kateřina Polášková[1,2] · David Nečas[1] · Lukáš Dostál[3] · Miloš Klíma[4] · Lenka Zajíčková[1,2]

✉ Lenka Zajíčková
lenkaz@physics.muni.cz

Kateřina Polášková
polaskova@vutbr.cz

David Nečas
david.necas@ceitec.vutbr.cz

Lukáš Dostál
dostall@feec.vutbr.cz

Miloš Klíma
klimam@vut.cz

[1] Plasma Technologies, Central European Institute of Technology - CEITEC, Brno University of Technology, Purkyňova 123, Brno CZ-61200, Czech Republic

[2] Department of Condensed Matter Physics, Faculty of Science, Masaryk University, Kotlářská 2, Brno CZ-61137, Czech Republic

[3] Department of Power Electrical and Electronic Engineering, Faculty of Electrical Engineering and Communication, Brno University of Technology, Technická 12, Brno CZ-61600 Brno, Czech Republic

[4] Department of Theoretical and Experimental Electrical Engineering, Faculty of Electrical Engineering and Communication, Brno University of Technology, Technická 12, Brno CZ-61600 Brno, Czech Republic